Determining partial photoemission cross sections of methane with dedicated uncertainties

Hans Kirschner, Alexander Gottwald, Hendrik Kaser, and Mathias Richter
Physikalisch-Technische Bundesanstalt, 10587 Berlin, Germany

(Received 19 December 2023; accepted 5 April 2024; published 30 April 2024)

Photoemission spectroscopy is used to quantitatively determine the partial cross section of the $1t_2$ and $2a_1$ subshells of methane. Photoelectron spectra are recorded using a hemispherical electron analyzer and monochromatized synchrotron radiation. The corresponding emission peaks are analyzed to calculate the partial cross sections with the associated uncertainties in a photon energy range from 16.5 to 70 eV. The presented results cover this broad energy range with corresponding uncertainties and belong to the framework of photoemission orbital tomography, aiming to bridge the experimental gap between simple single atoms and complex molecular monolayers.

DOI: 10.1103/PhysRevA.109.042827

I. INTRODUCTION

In this paper, we present partial photoionization cross sections (PCSs) of methane (CH_4) on an absolute scale with assigned uncertainties from photoelectron emission spectra (PESs). CH_4 is a chemical compound with relevance in various domains such as combustion processes and climatology. Our key focus is on the characterization of ordered molecular monolayers on crystal surfaces using angular and photon energy-dependent photoemission techniques. With photoemission orbital tomography (POT), properties such as the charge transfer [1], molecular geometry [2,3], reaction intermediates [4], and molecular orbitals [5–7] have been quantified in recent experiments. Particularly impressive is the application of POT in reconstructing two- and three-dimensional real-space molecular orbitals from measurements in momentum space [8–10]. Although these results are remarkable, they lack absolute units (e.g., in terms of the electron density) since the absolute determination of all relevant quantities and the straightforward uncertainty estimation for such a complex experiment has been shown to be infeasible. However, a calibration standard could help to overcome this limitation.

Very recently, the POT formalism was extended to gas-phase atoms [11]. In particular, the radial electron densities for neon subshells were successfully reconstructed on an absolute scale with uncertainties, from absolute PCS data for $1s$, $2s$, and $2p$ subshells. However, a noble gas is not suitable as a calibration standard for the POT apparatus, as its preparation as a single surface layer is not feasible. A possible replacement for neon is CH_4, which has the same number of electrons in its electronic shell, with a comparable electronic level structure and assignment. Thus, the previously mentioned absolute reconstruction of radial electron densities may be transferable. Additionally, CH_4 is easily available and the preparation as a single monolayer on a surface is in principle possible [12–21]. Hence, CH_4 is a potential bridge from studying single atoms to more complex molecules in particular on surfaces.

To reconstruct absolute radial electron densities of CH_4, the availability of reliable absolute PCS data available with uncertainties is required. While absolute PCS data with trusted uncertainties for neon atoms are well known from the literature [22], the most recent data for methane dates back to the 1970s [23,24], is confined in the energy range, and offers only fragmentary uncertainties. Nevertheless, these dated values are still referenced in recent studies on PCS calculations [25–27].

We attempt to obtain reliable absolute PCS data of the CH_4 states $1t_2$ and $2a_1$ from PESs with detailed uncertainties, using monochromatized synchrotron radiation. The spectra are recorded in the photon energy range from 16.5 to 70 eV, exceeding the energy range from the literature. The resulting PCSs are scaled to already known total photoionization cross sections [28] to obtain absolute units.

II. EXPERIMENT

The measurements were conducted at the Insertion Device Beamline of the Metrology Light Source [29], where linearly polarized and monochromatic synchrotron radiation in the photon energy range between 14 and 120 eV is supplied [30–32]. The photon energy scale is calibrated, using photoabsorption resonances of noble gases [31]. The beamline is capable of providing an absolutely measured photon flux $\Phi(h\nu)$, necessary for a reliably quantitative determination of the photon-energy-dependent PCS. Thus, care must be taken in the evaluation of $\Phi(h\nu)$, which is measured by means of traceably calibrated reference detectors, i.e., silicon-based photodiodes. These diodes would block the photon beam during the experiment. In practice, the photon flux is therefore monitored by a photoemission current monitor from the last beamline mirror. For each energy step and independently of the actual experiment, its mirror current $I_M(h\nu)$ is measured and its photon yield $\eta(h\nu)$ is calibrated to the reference diodes. These two measurands are related to the photon flux via $\Phi(h\nu) = I_M(h\nu)\eta(h\nu)$. During the experiment, the photon flux is then monitored by the mirror current I_M.

The PESs were measured with a SCIENTA R4000 hemispherical electron spectrometer [33] under an angle of 45° relative to the polarization axis of the synchrotron radiation.

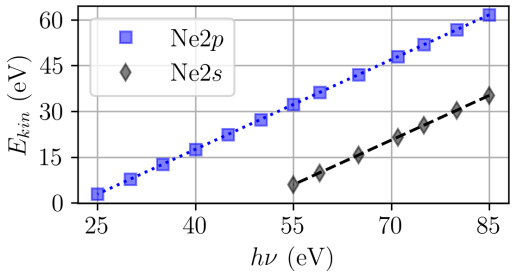

FIG. 1. Energy scale calibration, using Eq. (1) to fit the peaks from neon $2p$ and $2s$ for different photon energies $h\nu$, represented by markers ■ and ♦, respectively. The lines mark the fit function (1).

The pass energy was set to 5 eV and a slit of 800 was chosen, which corresponds to a slit width of 2.5 mm and a slit length of 30 mm. A titanium tube with an inner diameter of 0.35 mm was used as the gas inlet to the analyzer chamber and the pressure was carefully monitored using dedicated gauges to ensure stability throughout the experiment. The purity of the utilized CH_4 was 99.95%.

III. PHOTOELECTRON SPECTRA AND BINDING ENERGIES OF CH_4

Before analyzing the measured spectra, it is necessary to calibrate the energy scale of the spectrometer to achieve comparable results. We use the well-known binding energies of neon $2s$ and $2p$ [34] as reference points.

The relation between the photon energy $h\nu$, the binding energy E_B of the respective state, and the kinetic energy E_{kin} is $E_{\text{kin}} = h\nu - E_B$, which defines the energy scale between $h\nu$ and E_{kin} as a linear function. While measuring the $2s$ and $2p$ peaks of neon for different photon energies $h\nu$, deviations in the form of a linear shift of the energy scale are noticeable. This effect can be explained with a deviation of the applied voltage at the input lens of the spectrometer from the preset value, which controls the E_{kin} of the incoming photoelectrons. We apply a corrective function

$$E_{\text{kin}} = (1+m)h\nu + a - E_B, \tag{1}$$

with m an additional slope to unity and a the offset. Equation (1) is fitted to the peak positions of neon $2s$ and $2p$ to evaluate the parameters m and a as the mean of both fits to $m = -2.1(2) \times 10^{-2}$ and $a = 0.1(1) \times 10^{-1}$ eV (see Fig. 1). Since just the slope m is of significant magnitude, we only apply this value to correct the energy scale for each CH_4 spectrum.

TABLE I. Binding energy E_B of the CH_4 states $2a_1$ and $1t_2$ obtained in the present paper compared to literature values [36].

	E_B (eV)	
State	Ref. [36]	This work
$2a_1$	23.0(4)	22.8(1)
$1t_2$	14.5(6)	14.5(1)

An exemplary PES of CH_4 is shown in Fig. 2, which was acquired at a photon energy of $h\nu = 45$ eV. Two relatively broad structures are visible, which are assigned to the emission from the $2a_1$ and $1t_2$ states of CH_4. Figure 3 shows a series of spectra of the $2a_1$ and $1t_2$ emission for photon energies ranging from 16.5 eV ($1t_2$) and 28 eV ($2a_1$) up to 70 eV. All spectra are normalized to their respective maximum and plotted versus the binding energy.

To validate our measurements by the literature, we first estimate the binding energies E_B of both states and compare them to the results from Ref. [36], where E_B was provided with the full width at half maximum (FWHM). We use a FWHM equal to $\sqrt{8\ln 2}\,\hat{\sigma}$ to calculate the standard deviation $\hat{\sigma}$ as a comparable value to our uncertainty estimation.

For the $2a_1$ emission we estimate $E_B^{2a1} = 22.8$ eV from the mean of all maxima with a standard deviation of 0.09 eV. It can be seen from the spectra in Fig. 3, that the $1t_2$ peak is broadened by substructures. We recognize two maxima at about 13.5 and 14.5 eV, which can be assigned to the Jahn-Teller effect [35]. To evaluate the binding energy, we choose 14.5 eV, which is closer to the overall centroid of the $1t_2$ peak. We obtain $E_B^{1t2} = 14.5$ eV from the mean of all maxima with a standard deviation of 0.09 eV.

In addition to the standard deviation, we identify the Fermi-Dirac broadening of the spectrometer with a gold spectrum. As a fit function we apply a Fermi-Dirac distribution $f(E) \propto \{1 + \exp[-\hat{\beta}(E - E_F)]\}^{-1}$. The fit results in a broadening of $\hat{\beta}^{-1} \approx 0.05$ eV.

Together with the aforementioned standard deviations of 0.09 eV, we estimate the uncertainty values to 0.1 eV and present them with the evaluated binding energies in Table I. The results are in fair agreement with the literature [36].

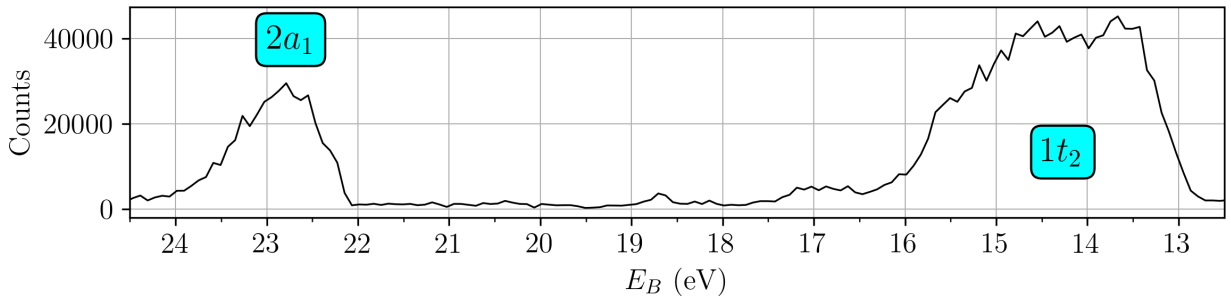

FIG. 2. PESs of CH_4 $2a_1$ and $1t_2$, measured at $h\nu = 45$ eV. The peaks $1t_2$ and $2a_1$ show an underlying structure, assigned to vibrational modes [35,36].

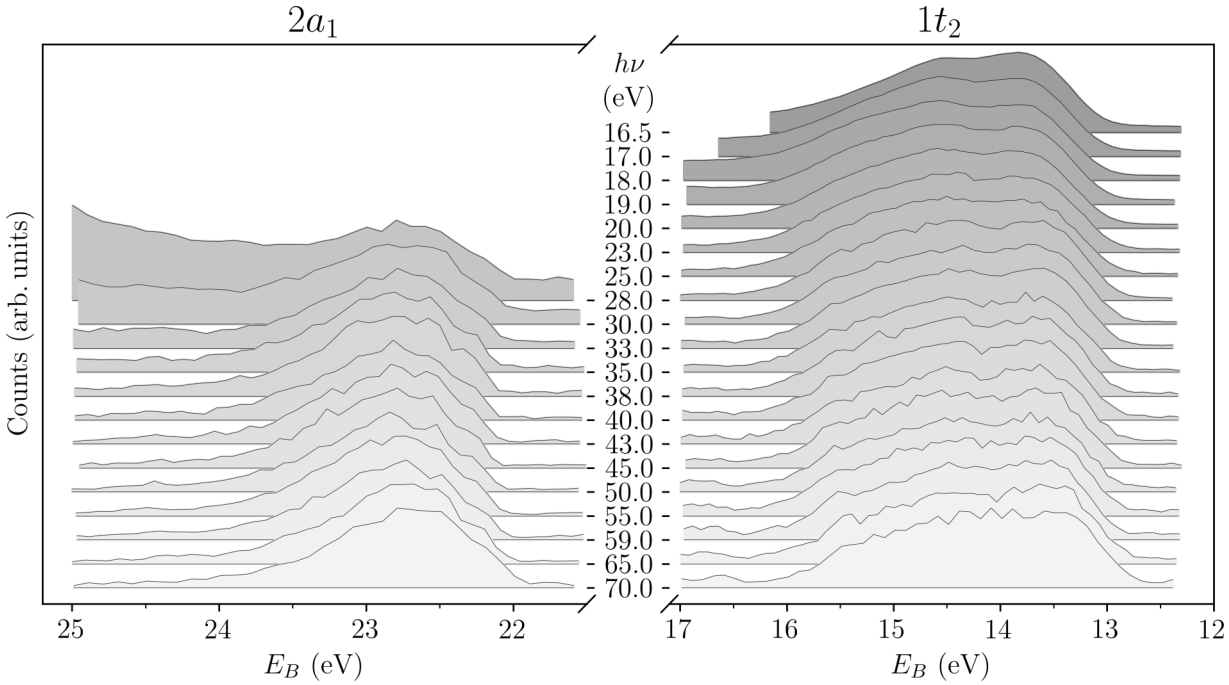

FIG. 3. Normalized PESs of the CH_4 peaks $2a_1$ and $1t_2$ for different photon energies $h\nu$.

IV. DETERMINATION OF PARTIAL CROSS SECTIONS OF CH_4 WITH UNCERTAINTIES

A. Partial-cross-section evaluation

The PCSs $\sigma_i(h\nu)$, with i denoting photoionization from a specific subshell i, are the constituent parts of the total photoionization cross section $\sigma_{\text{tot}}(h\nu) = \sum_i \sigma_i(h\nu)$. The latter can be measured on an absolute scale in units of megabarns and is known from the literature [28]. The PCSs $\sigma_i(h\nu)$ are measured on a relative scale and independently of $\sigma_{\text{tot}}(h\nu)$. Absolute units for the $\sigma_i(h\nu)$ are realized by scaling the experimental total photoionization cross section $\sigma_{\text{tot}}^{\text{expt}}(h\nu) = \sum_i \sigma_i(h\nu)$ to its equivalent from the literature $\sigma_{\text{tot}}^{\text{lit}}(h\nu)$ with a scaling factor B [22,37] via

$$\sigma_{\text{tot}}^{\text{lit}}(h\nu) = B\sigma_{\text{tot}}^{\text{expt}}(h\nu). \tag{2}$$

The energy- and angular-dependent differential PCS is given for linearly polarized light by [22,25,38]

$$\begin{aligned}\frac{d\sigma_i}{d\Omega} &= \sigma_i^{\Omega}(h\nu, \gamma) \\ &= \frac{\sigma_i(h\nu)}{4\pi}[1 + \beta_i(h\nu)P_2(\cos\gamma)],\end{aligned} \tag{3}$$

with $\sigma_i(h\nu)$ the PCS and $\beta_i(h\nu)$ the asymmetry parameter, describing the angular dependence. The angle between polarization and the wave vector of the radiation is represented by γ, and $P_2(x) = (3x^2 - 1)/2$ is the associated Legendre polynomial of the second degree.

Since the spectrometer is positioned at $\gamma = 45°$, we need to extract $\sigma_i(h\nu)$ from Eq. (3) via

$$\sigma_i(h\nu) = 4\pi \frac{\sigma_i^{\Omega}(h\nu, \gamma = 45°)}{1 + \beta_i(h\nu)P_2(\cos(45°))}. \tag{4}$$

The cross section σ_i^{Ω} at the angle of $\gamma = 45°$is measured by

$$\sigma_i^{\Omega}(h\nu) = \frac{1}{N\eta(h\nu)I_M(h\nu)} \frac{A(h\nu)}{nT(E_{\text{kin}})}, \tag{5}$$

where N is the number of measurement runs per spectrum, η the photon yield, $I_M(h\nu)$ the mirror current, A the area under the peak of the PES, n the particle density, and T the transmission function of the spectrometer.

B. Uncertainty analysis

In the following, we attempt to evaluate the associated measurement uncertainty contribution for each experimentally determined parameter in Eqs. (4) and (5), as precisely as possible in order to obtain a reliable total uncertainty for the final result.

1. Photon yield and mirror current

The photon yield $\eta(h\nu)$ is measured with photodiodes, whose detection efficiency and uncertainty vary with the photon energy $h\nu$. The maximum value for the uncertainty is about 6%.

The mirror current $I_M(h\nu)$ is measured with a dedicated amperemeter with a minuscule accuracy better than 0.01%. Per spectrum, $I_M(h\nu)$ is read out only once and approximated to be constant over the typical measurement time of 10 min. However, the ring current of the storage ring and thus the resulting photon flux decays over time, leading to a deviation in the readout of $I_M(h\nu)$, which is estimated to 1% and thus defines the uncertainty for $I_M(h\nu)$.

2. Relative particle density

The relative particle density n is proportional to the pressure p inside the vacuum chamber, which was measured with

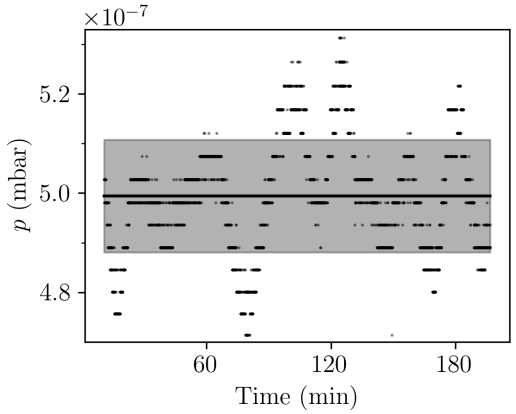

FIG. 4. Example of the pressure p during the acquisition of the PES. The solid line gives the mean value, while the shaded area denotes the standard deviation.

a Pfeiffer PBR 260 gauge and maintained at a constant value with a needle valve, showing minor fluctuations. Figure 4 shows a typical example for the pressure data over 180 min during the measurement of the PES series. The distinct steps in the data are due to the resolution of the pressure gauge. The mean value is $p = 4.99 \times 10^{-7}$ mbar with a relative uncertainty of about 2%. For this limited range of pressure measurement, the factor between the particle density n and the pressure p can be reasonably assumed to be constant and is later tacitly included to the scaling factor B in Eq. (2).

3. Relative peak area

To consistently evaluate the area A of each spectrum, the baseline is subtracted systematically, by fitting a model of skew-normal distributions with a polynomial background to the spectra. As an example, Fig. 5(a) shows the $1t_2$ spectrum gained at a photon energy of $h\nu = 19$ eV. These estimations are merely a means to an end, aiming to determine

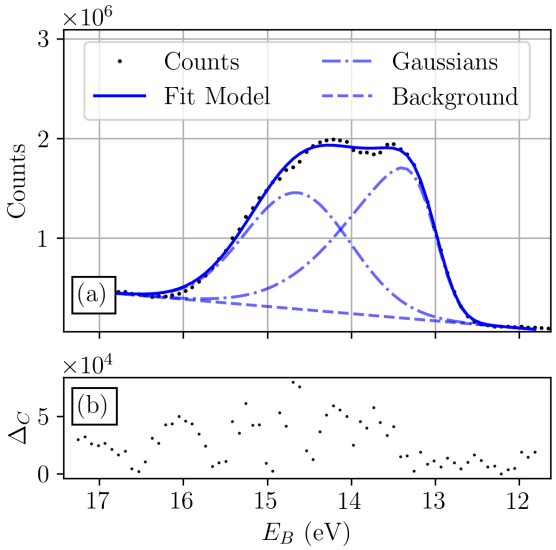

FIG. 5. (a) Spectrum and fit of the CH_4 $1t_2$ peak, assessed at $h\nu = 19$ eV. (b) Absolute deviation Δ_C of the measured counts to the fit.

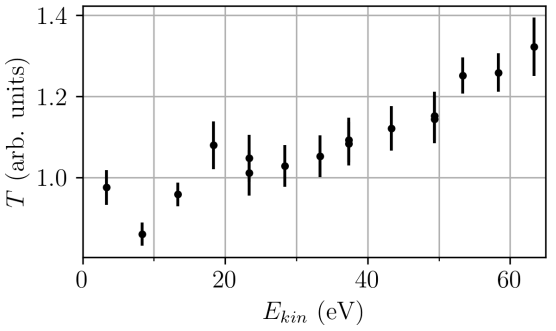

FIG. 6. Relative spectrometer transmission function $T(E_{\text{kin}})$ for kinetic electron energies up to 65 eV with uncertainties.

the background as consistently as possible for all spectra, as the actual peaks are much more complex, due to the vibrational modes [35,36]. Despite this simplification, we could obtain comparable small deviations $\Delta_C = |\text{fit} - \text{counts}|$ of about two magnitudes less than the actual count rate, as shown in Fig. 5(b).

The area A beneath each spectrum is assessed by numerical integration after subtracting the background, acquired from the fitting process. The relative uncertainty of A is estimated via $\sum \Delta_C/A$ to less than 0.1%.

4. Relative spectrometer transmission

The relative transmission T of the spectrometer is determined using neon with its $2p$ state as a reference gas, for which the cross section $\sigma_{\text{Ne}\,2p}$ [39,40] and the asymmetry parameter $\beta_{\text{Ne}\,2p}$ [37,41–44] plus their respective uncertainties of less than 5% are well known.

To obtain $T(E_{\text{kin}})$, Eqs. (4) and (5) are rearranged to

$$T(E_{\text{kin}}) = \frac{1}{N\eta(h\nu)I_M(h\nu)}\frac{A(h\nu)}{n} \times \frac{4\pi}{1+\beta_{\text{Ne}\,2p}P_2(\cos(45^\circ))}\frac{1}{\sigma_{\text{Ne}\,2p}(h\nu)}. \quad (6)$$

The parameters η, A, I, and n and their uncertainties are evaluated similarly to those of the measurements for CH_4, as described before. The relative uncertainty contribution of the relative spectrometer transmission is estimated to about 5%. Figure 6 shows the relative transmission function with uncertainties up to about $E_{\text{kin}} = 65$ eV.

5. Asymmetry parameter β

An angular correction with the asymmetry parameter according to Eq. (4) is in general necessary to calculate the PCS. In the following we write just β instead of β_i.

For photoionization of spherically symmetric s-like states like the $2a_1$ state, β is constant and equal to 2 [38]. Thus, a correction to β is not necessary and Eq. (4) can be simplified to $\sigma_i(h\nu) \propto \sigma_i^{\Omega}(h\nu)$.

For states other than s-like states, however, this is not the case. Experimental data for β of the $1t_2$ state in CH_4 are available up to 30 eV with uncertainties from Marr and Holmes [45]. Above 30 eV, no experimental data could be found in the literature. Although calculated data are available in principle [46], these however only match the experimental data

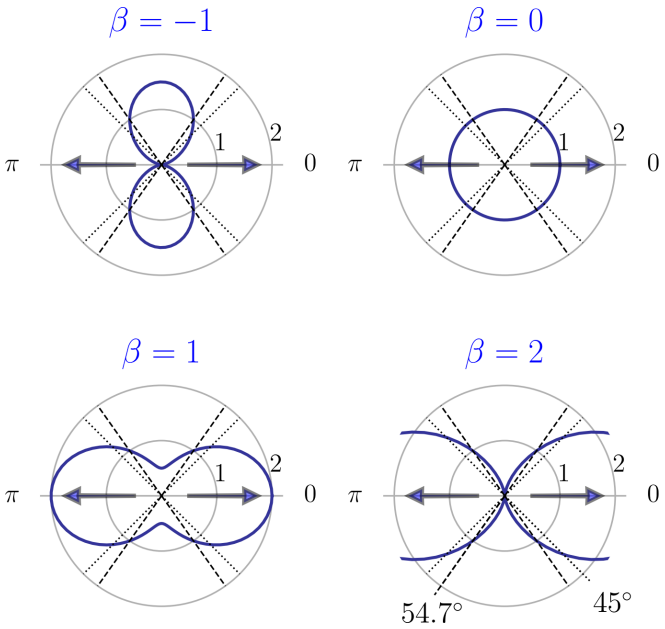

FIG. 7. Angular distribution for different values of the asymmetry parameter β, presented by the solid curved line. The arrows mark the direction of the linear polarization. The scaling is such that 1 equals the PCS $\sigma_i(h\nu)/4\pi$. The straight lines mark angles of 45° (· · ·) and 54.7° (- - -).

qualitatively. They also come without an uncertainty, which is essential for this work. Thus, we introduce an estimation for β and its uncertainty instead, using the following method, which covers the mentioned calculated results from [46].

The angular part in Eq. (3) is

$$\Theta(h\nu, \gamma) = 1 + \beta(h\nu)P_2(\cos\gamma), \tag{7}$$

where β can take values between -1 and 2 [38]. We plot Θ for different β in Fig. 7. At the so-called magic angle of 54.7°, Eq. (7) becomes $\Theta(h\nu) = 1$ and the angular dependence of Eq. (3) vanishes, leading to $\sigma_i^\Omega = \sigma_i$. Measuring at a different angle than the magic angle will introduce a deviation Δ from $\sigma_i(h\nu)$ for any $\beta \neq 0$, which is used to estimate the uncertainty for 45° via

$$\begin{aligned}\Delta &= \left|\sigma_{1t2}^\Omega(45°)/\sigma_{1t2}^\Omega(54.7°) - 1\right| \\ &= |\Theta(h\nu, \gamma = 45°) - 1|.\end{aligned} \tag{8}$$

From the plots in Fig. 7 it can be seen that Δ is equal to zero for $\beta = 0$ and peaks for $\beta = 2$. In [45] the last β value at $h\nu = 30$ eV is $\beta \approx 0.9$. We approximate the course of β above 30 eV up to 70 eV as a constant of $\beta = 1$ and estimate the uncertainty to $\Delta_{\beta=1} = 0.25$, according to Eq. (8) and Fig. 7. These β values are plotted together with the values from [45,46] in Fig. 8.

To calculate the total uncertainty for $\sigma_i(h\nu)$, we use propagation of uncertainty and neglect covariances

$$u_{\sigma_i}^2 = \sum \left(\frac{\partial\sigma_i}{\partial x_k} u_{x_k}\right)^2, \tag{9}$$

with x_k denoting the variables of σ_i and u_{x_k} denoting its uncertainty. For η, I_M, A, n, and T the term in large parentheses

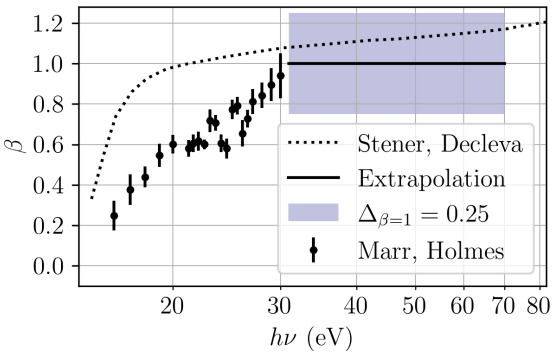

FIG. 8. Parameter β for σ_{1t2} as taken from Marr and Holmes [45] up to 30 eV (•) with uncertainties. Above 30 eV we extrapolate $\beta = 1 \pm 0.25$ (— and shaded area). The calculated values from Stener and Decleva [46] are included for comparison (· · ·).

simply becomes a multiplication of $\sigma_i(h\nu)$ with the relative uncertainty $u_{x_k}^{\text{rel}} = u_{x_k}/x_k$. However, for β we get, from Eq. (4),

$$\left(\frac{\partial\sigma_i}{\partial\beta}u_\beta\right)^2 = \left(u_\beta \frac{\partial}{\partial\beta}\frac{\sigma_i^\Omega}{1+\beta P_2(\cos\gamma)}\right)^2 \tag{10}$$

$$= \left(\frac{P_2(\cos\gamma)}{1+\beta P_2(\cos\gamma)} u_\beta \sigma_i\right)^2 \tag{11}$$

$$= \left(\hat{u}_\beta^{\text{rel}}\sigma_i\right)^2. \tag{12}$$

Here $\hat{u}_\beta^{\text{rel}}$ can be treated as a relative uncertainty of β, which comes in handy in calculating the total uncertainty for σ_i (see the next section). In the range below 30 eV, $\hat{u}_\beta^{\text{rel}}$ is 1%. Above 30 eV the value increases to 6.3%.

6. *Resulting total measurement uncertainty*

With the notation of $\hat{u}_\beta^{\text{rel}}$ in Eq. (12), Eq. (9) simply becomes the sum of all squared relative uncertainties $(u_{\sigma_i}^{\text{rel}})^2 = \sum_k (u_{x_k}^{\text{rel}})^2$. Table II provides a summary of all relative uncertainties for exemplary energies.

The largest contribution for $1t_2$ arises from β with a value of 6.3%. The second highest contribution is added by the photon yield, amounting to approximately 6.1%. For $2a_1$, the highest contributions result from the spectrometer transmission.

TABLE II. Exemplary relative standard uncertainties for σ_{2a1} and σ_{1t2} for the $h\nu = 20$, 30, and 40 eV.

		Relative uncertainty (%)						
$h\nu$ (eV)	Orbital	p	I_M	A	T	η	β	$\sum$
20	$1t_2$	2.1	1.0	0.1	3.7	6.1	1.0	7.6
30	$1t_2$	2.4	1.0	0.1	4.5	0.8	1.0	5.4
	$2a_1$	2.4	1.0	0.1	3.3	0.8		4.3
40	$1t_2$	1.0	0.1	0.1	5.2	0.8	6.3	8.6
	$2a_1$	1.0	0.1	0.1	5.4	0.8		6.1

C. Absolute partial cross sections

To obtain the absolute PCS, the relative data of the photoionization cross section has to be scaled to absolute data. Usually, for such a scaling the Thomas-Kuhn-Reiche sum rule is used, which however only holds for absolute photoabsorption data [47–49]. Instead, we scale the relative photoionization data to the total photoionization data from the literature $\sigma_{\mathrm{tot}}^{\mathrm{lit}}$ [28], as explained in Sec. IV A. Up to 28 eV, the total photoionization of CH_4 is the sum of the main peaks from the $1t_2$ and $2a_1$ molecular orbitals. Starting from 29 eV, additional satellite states need to be taken into account [24,36,50], which are not considered in this work.

The scaling factor B from Eq. (2) is estimated from individual factors B_j, evaluated for each photon energy $h\nu_j$ up to 28 eV. These factors are determined by

$$B_j = \frac{\sigma_{\mathrm{tot}}^{\mathrm{lit}}(h\nu_j)}{\sigma_{\mathrm{tot}}^{\mathrm{expt}}(h\nu_j)}. \tag{13}$$

The overall scaling factor B is finally evaluated from the weighted average of the individual factors B_j via

$$B = \frac{\sum_j w_j B_j}{\sum_j w_j}. \tag{14}$$

Here the weightings are calculated from the uncertainties u_j of the respective B_j factors via $w_j = \frac{1}{u_j^2}$. The uncertainties u_j are calculated from error propagation of Eq. (13). The units of B are megabarns per arbitrary units, thus assigning absolute units of megabarns to the experimental data, initially given in arbitrary units. The estimated value of B is assumed to be constant, to exceed the starting point for the satellites at a photon energy of 29 eV. The resulting data for σ_{1t2} and σ_{2a1} are summarized in Table III in comparison with the literature data.

1. Subshell $1t_2$

The results for $1t_2$ are summarized in Fig. 9(a), where σ_{1t2} is marked with pluses plus uncertainties. Literature values for σ_{1t2} are included from Backx and Wiel [24] (triangles) and Wiel *et al.* [23] (crosses) for comparison, together with $\sigma_{\mathrm{tot}}^{\mathrm{lit}}$. The latter is represented by a thin filled area, denoting the associated uncertainty range. Above 25 eV, the sum of σ_{1t2} and σ_{2a1} is additionally presented, marked by circles.

To better recognize differences, Fig. 9(b) shows the deviation between $\sigma_{\mathrm{tot}}^{\mathrm{lit}}$ and all other data, already presented in Fig. 9(a). Our σ_{1t2} data are presented in Figs. 9(a) and 9(b) with expanded uncertainties ($k = 2$) and agree fairly well with the data from the literature. Starting from $h\nu = 28$ eV, the sum of σ_{1t2} and σ_{2a1}, marked by circles, has to be compared to the literature data, as mentioned above. The associated uncertainties are omitted here, to maintain clarity in the figure; however, the main contribution to the sum's uncertainty stems from σ_{1t2}, resulting again in good agreement with $\sigma_{\mathrm{tot}}^{\mathrm{lit}}$.

2. Subshell $2a_1$

The PCS for $2a_1$ is approximately one order of magnitude smaller than for $1t_2$. Therefore, we present the results separately in Fig. 10, marked by circles and again with expanded uncertainties ($k = 2$), similar to Fig. 9. We again compare our

TABLE III. Summary of the results for the PCS of CH_4 $2a_1$ and $1t_2$ and the total cross section $\sigma_{\mathrm{tot}}^{\mathrm{lit}}$ from [28]. Uncertainties are given as expanded uncertainties with expansion factor $k = 2$ with 95% confidence.

$h\nu$ (eV)	σ_{tot} (Mb)	σ_{1t2} (Mb)	σ_{2a1} (Mb)
16.5	44.63(3.79)	47.27(7.68)	
17	43.24(3.67)	53.49(8.64)	
18	39.92(3.39)	48.77(7.69)	
19	37.08(3.15)	40.67(6.29)	
20	34.39(2.92)	36.78(5.59)	
23	26.32(2.23)	25.42(2.87)	
25	22.06(1.87)	20.03(2.22)	
28	16.95(1.44)	14.23(1.31)	1.03(0.10)
30	14.03(1.19)	12.03(1.29)	1.17(0.10)
33	10.76(0.91)	10.03(1.75)	1.12(0.09)
35	9.20(0.78)	8.29(1.45)	1.25(0.10)
38	7.38(0.63)	5.94(1.03)	1.21(0.13)
40	6.42(0.54)	4.98(0.85)	1.19(0.14)
43	5.24(0.44)	3.93(0.66)	1.09(0.13)
45	4.67(0.40)	3.46(0.58)	0.95(0.12)
50	3.54(0.30)	2.59(0.44)	0.79(0.09)
55	2.71(0.23)	1.74(0.29)	0.63(0.07)
59	2.22(0.19)	1.48(0.25)	0.57(0.06)
65	1.71(0.15)	1.11(0.18)	0.45(0.05)
70	1.39(0.12)	0.90(0.14)	0.40(0.05)

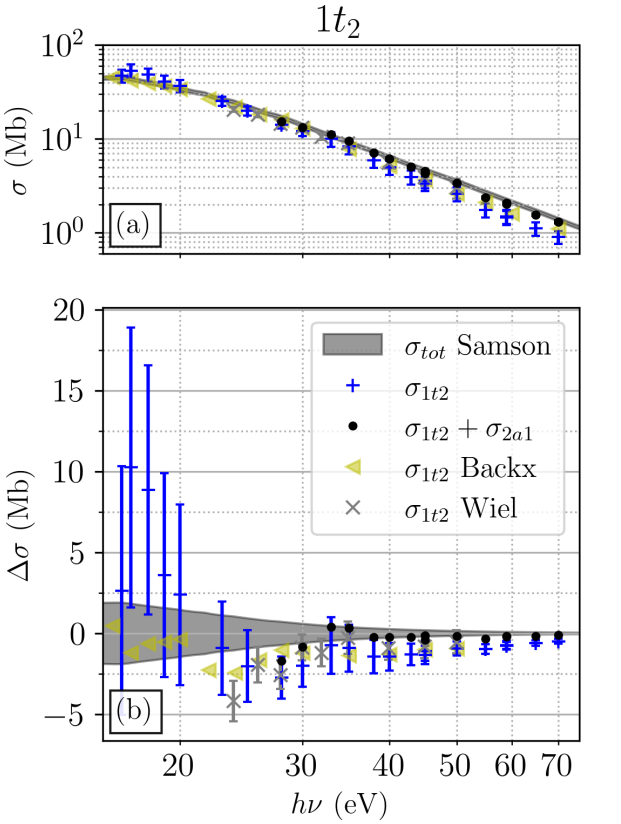

FIG. 9. PCS results for CH_4 $1t_2$ (+) with error bars representing the expanded uncertainties ($k = 2$). Literature data from Backx and Wiel [24] (◀), Wiel *et al.* [23] (×) and $\sigma_{\mathrm{tot}}^{\mathrm{lit}}$ [28] (shaded area) are shown for comparison. The data of $2a_1$ are added for photon energies $h\nu \geqslant 28$ eV (•) as the sum $\sigma_{1t2} + \sigma_{2a1}$. (a) A log-log plot of cross sections. (b) Difference $\Delta\sigma$ plotted with $\sigma_{\mathrm{tot}}^{\mathrm{lit}}$ as reference.

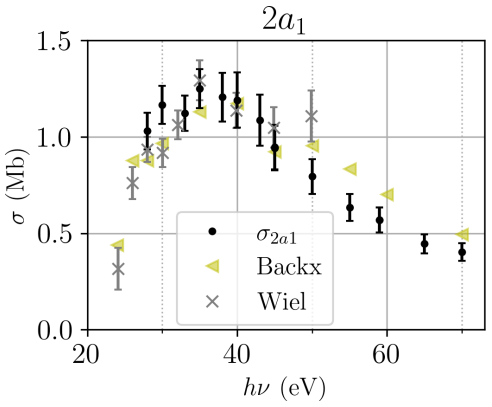

FIG. 10. PCS results for CH_4 $2a_1$ (•) with expanded uncertainties ($k = 2$). Literature data from Backx and Wiel [24] (◀) and Wiel *et al.* [23] (×) are shown for comparison.

findings with the data from [23,24]. Below 50 eV, our data align well with these values.

Above 50 eV deviations of the presented results from the data of Backx and Wiel [24] are visible, but a reliable comparison is problematic due to missing uncertainties from the literature data. However, at 50 eV, Wiel *et al.* [23] reported a value for σ_{2a1} at approximately 1.1 Mb, following the trend of the data of Backx and Wiel. We believe this correlation is due to the similar experimental methods of Backx and Wiel, using electron impact measurements.

V. CONCLUSION

We evaluated the PCSs for the CH_4 $2a_1$ and $1t_2$ states from PESs. The obtained binding energies of the $2a_1$ and $1t_2$ states are in fair agreement with the literature values. Further, PCSs were extracted along with their associated uncertainties in a photon energy range from 16.5 to 70 eV, which is an improvement on the literature data, which do not provide any uncertainty at all or are restricted in the energy range.

The experiments conducted in this study belong to the framework of POT, aimed at a deeper understanding of the photoemission process in CH_4 with the general purpose of being used for molecular orbital reconstruction. Absolute PCS measurements with uncertainties serve as a next step to produce quantifiable results within POT and to promote it as a reliable experimental method.

Future improvements to the experiment may involve installing the spectrometer at the magic angle of 54.7°. Thereby, the need for the correction by the asymmetry parameter β is eliminated and leads to enhanced accuracy and increased reliability in the measurements for the transmission function and the PCS itself.

ACKNOWLEDGMENTS

This work was funded by the Exploring the Foundations of Photoemission Tomography project of the DFG Project No. 396769409 and FWF with Project No. I 3731, respectively.

[1] P. Hurdax, M. Hollerer, P. Puschnig, D. Lüftner, L. Egger, M. Ramsey, and M. Sterrer, Adv. Mater. Interfaces **7**, 2000592 (2020).
[2] P. Hurdax, M. Hollerer, L. Egger, G. Koller, X. Yang, A. Haags, S. Soubatch, F. Tautz, M. Richter, A. Gottwald, P. Puschnig, M. Sterrer, and M. Ramsey, Beilstein J. Nanotechnol. **11**, 1492 (2020).
[3] D. Lüftner, M. Milko, S. Huppmann, M. Scholz, N. Ngyuen, M. Wießner, A. Schöll, F. Reinert, and P. Puschnig, J. Electron. Spectrosc. Relat. Phenom. **195**, 293 (2014).
[4] X. Yang, L. Egger, P. Hurdax, H. Kaser, D. Lüftner, F. C. Bocquet, G. Koller, A. Gottwald, P. Tegeder, M. Richter, M. G. Ramsey, P. Puschnig, S. Soubatch, and F. S. Tautz, Nat. Commun. **10**, 3189 (2019).
[5] M. Dauth, T. Körzdörfer, S. Kümmel, J. Ziroff, M. Wiessner, A. Schöll, F. Reinert, M. Arita, and K. Shimada, Phys. Rev. Lett. **107**, 193002 (2011).
[6] P. Puschnig, E.-M. Reinisch, T. Ules, G. Koller, S. Soubatch, M. Ostler, L. Romaner, F. S. Tautz, C. Ambrosch-Draxl, and M. G. Ramsey, Phys. Rev. B **84**, 235427 (2011).
[7] T. Ules, D. Lüftner, E. M. Reinisch, G. Koller, P. Puschnig, and M. G. Ramsey, Phys. Rev. B **90**, 155430 (2014).
[8] P. Puschnig, S. Berkebile, A. J. Fleming, G. Koller, K. Emtsev, T. Seyller, J. D. Riley, C. Ambrosch-Draxl, F. P. Netzer, and M. G. Ramsey, Science **326**, 702 (2009).
[9] S. Weiß, D. Lüftner, T. Ules, E. M. Reinisch, H. Kaser, A. Gottwald, M. Richter, S. Soubatch, G. Koller, M. G. Ramsey, F. S. Tautz, and P. Puschnig, Nat. Commun. **6**, 8287 (2015).
[10] M. Graus, C. Metzger, M. Grimm, P. Nigge, V. Feyer, A. Schöll, and F. Reinert, Eur. Phys. J. B **92**, 80 (2019).
[11] H. Kirschner, A. Gottwald, V. Soltwisch, M. Richter, P. Puschnig, and S. Moser, Phys. Rev. A **109**, 012814 (2024).
[12] M. Sakurai, T. Okano, and Y. Tuzi, Jpn. J. Appl. Phys. **26**, L1651 (1987).
[13] D. Meixner and S. M. George, Surf. Sci. **297**, 27 (1993).
[14] Y. A. Gruzdkov, K. Watanabe, K. Sawabe, and Y. Matsumoto, Chem. Phys. Lett. **227**, 243 (1994).
[15] D. J. Alberas-Sloan and J. White, Surf. Sci. **365**, 212 (1996).
[16] Y. Matsumoto, Y. A. Gruzdkov, K. Watanabe, and K. Sawabe, J. Chem. Phys. **105**, 4775 (1996).
[17] K. Watanabe, K. Sawabe, and Y. Matsumoto, Phys. Rev. Lett. **76**, 1751 (1996).
[18] T. Fuhrmann, M. Kinne, B. Tränkenschuh, C. Papp, J. F. Zhu, R. Denecke, and H.-P. Steinrück, New J. Phys. **7**, 107 (2005).
[19] H.-P. Steinrück, T. Fuhrmann, C. Papp, B. Tränkenschuh, and R. Denecke, J. Chem. Phys. **125**, 204706 (2006).
[20] Y. Tsuji and K. Yoshizawa, J. Phys. Chem. C **122**, 15359 (2018).
[21] H. Zhang, S. J. Tan, L. Prasetyo, D. D. Do, and D. Nicholson, Phys. Chem. Chem. Phys. **22**, 17134 (2020).
[22] *VUV and Soft X-Ray Photoionization*, edited by U. Becker and D. A. Shirley, Physics of Atoms and Molecules (Springer, New York, 1996).
[23] M. J. Wiel, W. Stoll, A. Hamnett, and C. E. Brion, Chem. Phys. Lett. **37**, 240 (1976).
[24] C. Backx and M. J. Wiel, J. Phys. B: At. Mol. Phys. **8**, 3020 (1975).

[25] N. M. Novikovskiy, V. L. Sukhorukov, A. N. Artemyev, and P. V. Demekhin, Eur. Phys. J. D **73**, 79 (2019).
[26] N. M. Novikovskiy, D. V. Rezvan, I. D. Petrov, B. M. Lagutin, P. V. Demekhin, and V. L. Sukhorukov, Eur. Phys. J. D **73**, 83 (2019).
[27] W. J. Brigg, A. G. Harvey, A. Dzarasova, S. Mohr, D. S. Brambila, F. Morales, O. Smirnova, and J. Tennyson, Jpn. J. Appl. Phys. **54**, 06GA02 (2015).
[28] J. A. R. Samson, G. N. Haddad, T. Masuoka, P. N. Pareek, and D. A. L. Kilcoyne, J. Chem. Phys. **90**, 6925 (1989).
[29] A. Gottwald, R. Klein, R. Müller, M. Richter, F. Scholze, R. Thornagel, and G. Ulm, Metrologia **49**, S146 (2012).
[30] A. Gottwald, U. Kroth, M. Richter, H. Schöppe, and G. Ulm, Meas. Sci. Technol. **21**, 125101 (2010).
[31] A. Gottwald, H. Kaser, and M. Kolbe, J. Synchrotron Radiat. **26**, 535 (2019).
[32] M. D. Neumann, C. Cobet, H. Kaser, M. Kolbe, A. Gottwald, M. Richter, and N. Esser, Rev. Sci. Instrum. **85**, 055117 (2014).
[33] C. Lupulescu, T. Arion, U. Hergenhahn, R. Ovsyannikov, M. Förstel, G. Gavrila, and W. Eberhardt, J. Electron Spectrosc. Relat. Phenom. **191**, 104 (2013).
[34] *X-Ray Data Booklet*, edited by A. Thompson (Lawrence Berkeley National Laboratory, Berkeley, 2009).
[35] J. W. Rabalais, T. Bergmark, L. O. Werme, L. Karlsson, and K. Siegbahn, Phys. Scr. **3**, 13 (1971).
[36] M. C. Göthe, B. Wannberg, L. Karlsson, S. Svensson, P. Baltzer, F. T. Chau, and M.-Y. Adam, J. Chem. Phys. **94**, 2536 (1991).
[37] F. Wuilleumier and M. O. Krause, Phys. Rev. A **10**, 242 (1974).
[38] J. Cooper and R. N. Zare, *Lectures in Theoretical Physics: Atomic Collision Processes* (Gordon and Breach, New York, 1969), Vol. 11C, p. 317.
[39] J. Bizau and F. Wuilleumier, J. Electron Spectrosc. Relat. Phenom. **71**, 205 (1995).
[40] R. Schäfer, A. Gottwald, and M. Richter, J. Phys. B: At. Mol. Opt. Phys. **51**, 135004 (2018).
[41] S. H. Southworth, A. C. Parr, J. E. Hardis, J. L. Dehmer, and D. M. P. Holland, Nucl. Instrum. Methods Phys. Res. Sect. A **246**, 782 (1986).
[42] H. Derenbach, R. Malutzki, and V. Schmidt, Nucl. Instrum. Methods Phys. Res. **208**, 845 (1983).
[43] K. Codling, R. G. Houlgate, J. B. West, and P. R. Woodruff, J. Phys. B: At. Mol. Phys. **9**, L83 (1976).
[44] J. L. Dehmer and D. Dill, Phys. Rev. Lett. **35**, 213 (1975).
[45] G. V. Marr and R. M. Holmes, J. Phys. B: At. Mol. Phys. **13**, 939 (1980).
[46] M. Stener and P. Decleva, J. Electron Spectrosc. Relat. Phenom. **104**, 135 (1999).
[47] K. Kameta, N. Kouchi, M. Ukai, and Y. Hatano, J. Electron Spectrosc. Relat. Phenom. **123**, 225 (2002).
[48] J. W. Au, G. Cooper, G. R. Burton, T. N. Olney, and C. E. Brian, Chem. Phys. **173**, 209 (1993).
[49] C. Backx, G. R. Wight, and M. J. Wiel, J. Phys. B: At. Mol. Phys. **9**, 315 (1976).
[50] C. Backx, G. R. Wight, R. R. Tol, and M. J. Wiel, J. Phys. B: At. Mol. Phys. **8**, 3007 (1975).